Visible light activated photocatalytic degradation of tetracycline by a magnetically separable composite photocatalyst: graphene oxide/magnetite/cerium-doped titania

Muhan Cao[a], Peifang Wang[a], Yanhui Ao[a,*], Chao Wang[a], Jun Hou[a], Jin Qian[a]

Key laboratory of Integrated Regulation and Resource Development on Shallow Lakes, Ministry of Education, College of Environment, Hohai University, Nanjing, 210098, China

Abstract

In this study, magnetic graphene oxide-loaded Ce-doped titania (MGO-Ce-TiO_2) hybridized composite was prepared by a facile method. The as-prepared samples exhibited good adsorption capacity, high visible-light photoactive and magnetic separability as a novel photocatalyst in the degradation of tetracyclines (TC). The intermediate products and photocatalytic route of TC were proposed based on the analysis results of LC-MS. Moreover, the repeatability of the photoactivity with the use of MGO-Ce-TiO_2 was investigated in the multi-round experiments with the assistance of an applied magnetic field. Therefore, the prepared composite photocatalysts were considered as a kind of promising photocatalyst in a suspension reaction system, in which they can offer effectively recovery ability. The effect of MGO content on the photocatalytic performance was also studied, and an optimum content was obtained.

Keywords: Ce-doped TiO_2, Magnetically separable, Graphene oxide,

* Corresponding author. Tel./ fax: +86 25 83787330

E-mail address: andyao@hhu.edu.cn (Y.H. Ao)

Tetracyclines, Photocatalysis

1. Introduction

Antibiotics chemicals are one of the most widely used drugs in human and animal treatment against infections. However, these antibiotics are difficult to be metabolized completely and their residues are expelled through urine and feces to the environment [1-3]. In recent years, more and more residues of pharmaceutical antibiotics have been detected in the environmental samples, including surface water, sewage water and soils [4, 5]. They have been proven to be a new class of potential contaminants, which may be chronically toxic to human and animals, disrupt indigenous microbial populations and domesticate multi-resistant bacterial strains [6-8]. Consequently, removal of antibiotics has been a subject which is necessary and significant. Tetracyclines (TC), the second most common antibiotics, have been widely used in animal treatment, aquiculture and livestock industry. Furthermore, it is found that conventional biological method cannot decompose TC due to their antibacterial nature. How to eliminate TC from environment has attracted the public concern and scientific interest.

In the past decades, various technologies have been employed to remove and degrade TC, such as adsorption [9-11], electrochemistry [12, 13], ozonation [14, 15], and photocatalysis and so on. Among these methods, photocatalysis has been considered as a promising approach to thoroughly remove TC from water and wastewater. Titanium dioxide (TiO_2) has been the most studied photocatalysts owing to its high efficiency, low cost, low toxicity and physical and chemistry stability [16,

17]. It has been devoted into the application of removal of TC. Reyes et al. [18] found that TC was significant mineralized in the presence of TiO_2 (P25). Under UV light irradiation, about 50% of the initial concentration was eliminated after 10 min. Palominos et al. [19] investigated the photocatalytic performance of TiO_2 in the photo-oxidation of TC under simulated solar light. The optimal condition of the photoreaction system was also obtained, consisting of the pH and the dosage of TiO_2. Zhu et al. [20] reported the photocatalytic performance of nanosized TiO_2 under different conditions and firstly analyzed the intermediates and possible pathways in the photocatalytic degradation of TC by nanosized TiO_2. However, only being excited by UV light has been a restriction to TiO_2, which cannot take advantage of the visible light in the solar light. Many attempts have been made to prepare doped TiO_2 to improve the photocatalytic performance and/or extend the light adsorption region. Experimental evidence has disclosed that TC could be photodegraded by doped TiO_2 under visible light irradiation [21].

For nanosized TiO_2, it is difficult and requires high cost to separate it from the treated water. The TiO_2-coated magnetic nanoparticles have been proposed as a means to overcome the separation problems [22, 23]. The magnetic TiO_2 photocatalysts could suspend homogeneously in the solution and be separated easily from treated water by applying an external magnetic field. However, the magnetic TiO_2 composite showed a low photoactivity and a high level of photodissolution when TiO_2 nanoparticles directly depositing onto the surface of magnetic particles [24, 25]. Graphene, a new member of carbon materials, has been used as a support material for

photocatalysts owing to its unique physical structure, large surface area, superior electrical conductivity and excellent adsorption capacity [26, 27]. These graphene- and graphene oxide (GO)-based photocatalysts always exhibited an enhanced photoactivity than the pristine ones, mainly because graphene and GO could suppress the recombination of photo-induced electron-hole pairs [28, 29]. Therefore, Graphene and GO could be good candidates as support templates to preventing magnetic particles directly coating on the TiO_2 host.

Herein, for the first time, we prepared a magnetically separable Ce-doped TiO_2-GO composite with an enhanced photoactivity and recyclability. The synthetic process was completed at low temperature. TC was chosen as the targeted pollutant to determine the photocatalytic performance of the composite catalyst.

2. Experimental section

2.1. Preparation of Ce-doped TiO_2 sol

Ce-doped TiO_2 sol was prepared by a sol-gel method under low temperature. 50 mL of Tetrabutyl titanate (TBT) and a definite amount of $Ce(NO_3)_3$ were diluted in 16 mL of isopropanol. Then the mixture liquid was added dropwise into 400 mL of acid water (pH = 2) under vigorous stirring. Then, the solution was kept at 75 °C under reflux condition for 24 h. After static settlement overnight, the milky Ce-doped TiO_2 sol was obtained. The mass ratio of Ce/TiO_2 was 0.5%, 1%, 2% and 5%, respectively. The samples with Ce content of 1% exhibited the highest photoactivity towards methylene blue (not shown). Thus such optimized ratio of Ce was chosen in our experiment. The "Ce-TiO_2" in the following refers to the samples with the mass ratio

of Ce/TiO_2 = 1%.

2.2. Preparation of Ce-doped TiO_2-MGO hybrid photocatalyst

GO was prepared by a modified Hummers method [30]. Magnetic GO (MGO) was synthesized by a two-step method as described in our previous work [31]. A definite amount of MGO was dispersed in the Ce-doped TiO_2 sol by ultrasonic. Then, the mixture solution was dried in a rotatory evaporator at 60 °C under vacuum. The obtained powder was Ce-doped TiO_2-coated MGO composite photocatalyst. The mass ratio of Ce-doped TiO_2/MGO was 1%, 2%, 5%, 10% and 20%, respectively. The samples were denominated as MGO-Ce-TiO_2-1%, MGO-Ce-TiO_2-2%, MGO-Ce-TiO_2-5%, MGO-Ce-TiO_2-10% and MGO-Ce-TiO_2-20%, respectively.

2.3. Characterization

The crystalline phases of the as-prepared samples were obtained by a powder X-ray diffractometer (XRD, Shimadzu, XD-3A) over the 2θ range 10-70° with Cu Kα radiation (λ=0.15418 nm). The morphologies and structures of the composites were observed using a transmission electron microscopy (TEM, Hitachi, H-7650). The UV-vis diffuse reflectance spectra (DRS) of the samples were obtained by a UV-vis spectroscopy (Shimadzu, UV-3600). An electrochemical station (Chenhua Instruments, CHI660D) was used for the recording of the photocurrent signal of the samples in Na_2SO_4 solution. The Brunauer-Emmett-Teller (BET) surface area of the samples was obtained on a BET analyzer (Micrometers, ASAP2020).

2.4. Photocatalytic reactions

The photoactivity of the prepared photocatalysts was performed by examining the

photodegradation of TC under visible light irradiation by a 300 W Xe lamp (Beijing Zhongjiaojinyuan Technology Co., Ltd, CEL-HXF300) with a 400 nm cut-off glass filter. 50 mg of the photocatalysts was added into 100 mL of TC solution, whose initial concentration was 25 mg L^{-1}. Prior to illumination, the resultant suspension was placed in the dark under stirring for 60 min to reach the adsorption-desorption equilibrium. At given time intervals, an aliquot of suspension was withdrawn. The concentration of TC was determined by a high performance liquid chromatography (HPLC, Waters, e2695). The photocatalytic performance of TiO_2 (Degussa, P25) towards TC was also studied under visible light irradiation.

2.5. Analytical methods

The concentration of TC was analyzed by a HPLC (Waters, e2695) with a reversed-phase C18 column (4.6 mm×150 mm, 5 μm) at 25 °C. The wavelength of the UV-vis detector was set at 355 nm. Mobile phase was 0.01 M oxalic acid buffer (72%), methanol (8%) and acetonitrile (20%) with a flow rate at 1.0 mL min^{-1}. The standard curve showed a good linearity between the concentration of TC and the peak area responses (R^2=0.9999).

Identification of the intermediates in the photodegradation of TC was analyzed by a liquid chromatography-mass spectrometry (LC-MS, Agilent, 6460 Triple Quad LC/MS series) in electrospray positive ion mode (ESI+) equipped with a C18 column (2.1 mm×50 mm, 1.8 μm). The mobile phase was a mixture of acetonitrile and formic acid (0.1%) with a flow rate of 0.25 mL min^{-1}. The injection volume was 5.0 μL. The fragment voltage and capillary voltage was 135 V and 2800 V, respectively. MS was

scanned by mass range from m/z 50 to 800.

3. Results and discussion

3.1. Characterization of the catalysts

The crystal structure and crystalline quality of Ce-TiO_2 and MGO-Ce-TiO_2 samples were examined by XRD analysis and the diffractograms are shown in Fig. 1. All the samples had similar pattern, which was dominated by anatase phase. At 2θ = 25.4°, the samples exhibited a strong peak, which represented (101) anatase phase reflections [32]. A little peak at 2θ = 30.7° was also detected, which was indexed to (121) plane of brookite phase. Furthermore, the diffraction peaks at 2θ = 37.7°, 47.7°, 54.1° and 62.8° were corresponding to anatase phase [33]. For all samples, no obvious diffraction peak of cerium oxide, GO and Fe_3O_4 was observed, which might be due to the low content of Ce and MGO.

Fig. 2(a) presents a typical TEM micrograph of MGO. From the figure, the gauze-like GO shows its sheet structure and corrugated edges. It can be also seen that the Fe_3O_4 nanoparticles have a uniform distribution on the surface of GO. The size of Fe_3O_4 particles is ranging from 15 nm to 35 nm. In Fig. 2(b), the Ce-TiO_2 exhibits particle morphology with average diameter of 10 nm. They are depositing on the surface of GO or anchoring on Fe_3O_4 particles. The GO layers with large surface area could provide a substrate for the Ce-TiO_2 particles to decrease the aggregation.

Fig. 3 shows the UV-vis DRS spectra of the Ce-TiO_2 and MGO-Ce-TiO_2 composites. The Ce-TiO_2 exhibited an absorption threshold at ca. 425 nm, which for P25 is about 400 nm [34]. Higher visible-light absorbance was obtained for Ce-TiO_2

than P25. For MGO-Ce-TiO_2 composites, an obvious red shift in the absorption edge was observed, compared to the pristine Ce-TiO_2. This result indicated that the introduction of MGO could favor to narrow the band gap of Ce-TiO_2. It can be ascribed to the chemical bonding between Ce-TiO_2 and GO, which is similar to the case of carbon materials-loaded TiO_2 composites [34-36]. Furthermore, the absorption ability in visible light range was greatly enhanced correspondingly with the increase of the MGO content. It revealed that MGO-Ce-TiO_2 composite had a stronger absorbance than naked Ce-TiO_2, which could facilitate the photocatalytic performance to some extend.

3.2. Photocatalytic performance of the prepared catalysts towards TC

The photocatalytic activities of the samples for the degradation of TC were tested under visible light irradiation. The kinetic process of TC degradation in the presence of different samples was investigated. A pseudo first order kinetic model was used to describe the photocatalytic reaction as following:

$$\ln(C_0 / C) = kt \qquad (1)$$

where t is the reaction time, k is the apparent rate constant, C_0 and C is the concentration of TC at t = 0 and at reaction time t after irradiation. The apparent rate constant k is the basic kinetic parameter which can reflect the photoactivity for different samples [37].

The results of TC degradation are shown in Fig. 4 and Table 1. In a control experiment, the TC solution was irradiated under the visible light in the absence of any photocatalysts, and the disappearance of TC was negligible. Visible light

illumination in the presence of TiO_2 (P25) resulted in a very limited photocatalytic decomposition of TC. Therefore, the photocatalytic activity of undoped TiO_2 was extremely low under visible light irradiation. These results clearly indicated that the degradation of TC in the solution was caused by the photocatalytic reactions on Ce-doped TiO_2 under visible light illumination. It can be seen that all the MGO-Ce-TiO_2 composites presented better activities than Ce-doped TiO_2 under the same condition. The results also showed that an increasing in the MGO content could promote obviously the photoactivity of hybridized samples. When the MGO content was relatively low (<10%), the photocatalytic performance increased monotonously. However, when the MGO content exceeded 10%, the removal rate of TC decreased. According to the results of TC degradation, an optimal loading amount of MGO on the Ce-doped TiO_2 was approximately 10%.

3.3. Origin of photocatalytic activity enhancement of MGO-Ce-TiO_2 composites

The photocatalytic process of semiconductors is intrinsically determined by four factors of photocatalysts, that is, the adsorption capacity, the specific surface area, the electronic properties and the light absorption ability. The enhancement of MGO-Ce-TiO_2 nanocomposites in the photocatalytic reaction can be firstly attributed to the enhanced adsorptivity. The remaining concentration fractions of TC solution are shown as histograms after reaching the adsorption-desorption equilibrium by different samples, as shown in Fig. 5. The adsorption capacity of TC was enhanced by the presence of MGO. It can be also seen that the adsorption of TC molecules onto the MGO-Ce-TiO_2 composites enhanced with the increase of MGO content, and the

MGO-Ce-TiO_2-20% presented the best adsorptivity for TC. The adsorption may be driven by π-π stacking between pollutant molecules and the surface of GO [38, 39], thereby exhibited faster photodecomposition of contaminate. Under irradiation, the Ce-TiO_2 nanocrystals was excited and the photogenerated radicals could fast transfer to the molecules adsorbed on the GO and take part in degradation reactions. Thus the adsorption-desorption equilibrium was broken, and more molecules could transfer from the solution to the interface of GO and be mineralized through a series of redox reaction [34]. On the basis of the above discussion, we proposed that adsorption capacity of GO could appreciably facilitate the photocatalytic reaction compared to bare Ce-TiO_2.

Another important influence of GO in the composites was that it could provide large surface area for the photocatalysts due to its unique two-dimensional structure. This has been reported by many previous researches [40-43]. The BET surface area of the samples was also investigated, and the results are shown in Table 1. It showed that the surface area of the composites increased when the amount of MGO increased from 0 to 20%. The layer-structured GO favored the crystals distribute evenly and also prevented the aggregation, which could lead to an enhanced photocatalytic activity. On the other hand, larger surface area could provide an increasing interfacial contact between the pollutant molecules and Ce-TiO_2 nanoparticles, and thus offering more photo-reaction centers and accelerating the photocatalytic reaction.

The electrical properties of the obtained samples were investigated by testing the photocurrents under the visible light. The transient photocurrent responses of the

samples were measured by depositing each sample on a FTO electrode versus Ag/AgCl reference electrode in Na_2SO_4 solution. Fig. 6 shows the curves of photocurrent intensity versus time for the samples with several on-off cycles of visible light irradiation. Under illumination, the current appeared promptly and reached a relatively steady stage. When the irradiation was interrupted, the photocurrent immediately fell to zero. It can be seen that the MGO-Ce-TiO_2 hybridized composites exhibited much higher photocurrent densities than naked Ce-TiO_2. The GO was believed to play a significant role in the electron transfer under an external bias, because the incorporation of GO ensured higher electronic conductivity and hence accelerated the separation of photoinduced electron-hole pairs and prolonged the transfer of electrons. The mechanism was shown in Fig. 7. Obviously, the photocurrent of MGO-Ce-TiO_2-20% under visible light irradiation has been extremely enhanced as large as 6.6 times in comparison with Ce-TiO_2.

The light absorption ability is also an important influence factor in the photocatalytic reaction, especially for the visible light-induced photocatalytic process. From the above discussion about DRS result, the MGO-Ce-TiO_2 displayed distinctly enhanced visible-light absorption than bare Ce-TiO_2, and also exhibited a red shift in the absorption edge. However, the photoactivity of MGO-Ce-TiO_2 hybrid depressed when the content of MGO exceeded the optimal value 10%, which might be caused by “shielding effect” [44, 45]. The excess content of MGO may shade the light and deteriorate the photocatalytic performance. MGO-Ce-TiO_2-10% displayed the highest photoactivity because it kept a good balance in the above four aspects.

3.3. Reaction mechanism of TC by the prepared catalysts

To clarify the photodegradation pathway of TC in the presence of MGO-Ce-TiO_2 composites, LC-MS analysis was employed to identify the intermediate products in the photocatalytic process. According to the removal rate in Table 1, 83% of TC was detoxified within 60 min. Mass spectrometry revealed numerous intermediates derived from the photocatalytic degradation of TC, the results shown in Table 2 and Fig. 8. It can be seen that a prominent ion with m/z 445 and the retention time of 2.518 min was observed, and it was corresponding to the deprotonated TC molecular ion. On the other hand, the analysis permitted the recognition of some intermediate products, compounds with m/z value of 475, 400, 274, 238, 433, 301, 149, 438 and 210 formed during the photodecomposition of TC in the presence of MGO-Ce-TiO_2. In this work, the degradation intermediate products proposed are not completely consistent with the results of previous reports, which might be determined by the unique characteristic of MGO-Ce-TiO_2. Based on the photodegradation intermediate products and previous works, the decomposition pathways were proposed as shown in Fig. 9, which outlines three routes. Generally, in a photocatalytic reaction, active hydroxyl radicals •OH are formed through the photo-generated holes combined with OH^- and H_2O molecules. The •OH radicals were confirmed to play a very important role in the photodecomposition of organic pollutants, which could attack the organic compounds through indirect addition or substitution [20].

During the whole photodegradation process, the intermediates were mainly generated through two routes: the loss of functional group(s) and the open-ring

reactions [20, 46]. For Pathway I, the formation of Product 1 (m/z=400) was proposed to form via loss of N-methyl groups and dislodging hydroxyl group at the position C3, which was also reported by Niu et al. [47]. Product 1 was further degraded led to the generation of Product 2 (m/z=274) via loss of amino groups, because of breakage of naphthalene ring A [21]. Then Product 2 decomposed through the smash of ring B and the substitution of C-C single bond by hydroxyl group. The resulted Product 3 (m/z=238) produced the Product 6 (m/z=149) via formation of carboxyl and dislodging hydroxyl groups. For Pathway II, Product 4 (m/z=433) was stemmed from TC degradation via loss of one N-methyl group due to the low energy of N-C bond [45, 48, 49]. Afterwards, Product 4 might undergo breakage of ring A and dehydroxylation reaction at C6 by oxidation of the •OH radicals to yield Product 5 (m/z=301). For Pathway III, Product 7 (m/z=475) was formed from an initial 1, 3-dipolar cyclic addition towards C11a-C12 double-bond, a rearrangement with the •OH radicals at C12 [15, 20] and oxidation of N-methyl to N-aldehyde group [20]. Then Product 7 might be transferred to Product 8 (m/z=438) through dislodging N-C bond and hydroxyl-substitution reaction by the attack of •OH radicals. Product 8 was transferred into Product 9 (m/z=210) via loss of methyl and hydroxyl group at C6 and the rupture of C-C single bond leading to the breakage of ring A and B. Product 5 and Product 9 were also further oxidized to form Product 6, which might be the last by-product before complete mineralization in the reaction system.

3.4. Reusability of the prepared catalysts

The regeneration of TiO_2 was a key factor to develop the heterogeneous

photocatalysts for practical application. The used samples were isolated by a magnet and washed with water and ethanol for several times, and then added into the fresh TC solution to evaluate the stability of the samples. Fig. 10 shows satisfactory durability of the photoactivity for the MGO-Ce-TiO_2-10% in four cycles of TC photodecomposition. MGO-Ce-TiO_2-10% can still offer relatively high adsorption and photodegradation performance even after four cycles in comparison of in comparison with bare Ce-TiO_2 in the first cycle. This might be ascribed to the separation method, which could reduce the mass loss compared to conventional method like centrifugation, sediment and filtration. We also observed the nanostructures of MGO-Ce-TiO_2-10% after magnetic separation, as shown in Fig. 11(a). No obvious change have been seen, because Fe_3O_4 nanoparticles involved in our system show the superparamagnetic property, which can favor the composites re-disperse in the water after magnetic separation.

The gradual decrease of adsorption and photodegradation activity can be ascribed to two reasons. That is, small amounts of residual TC and other by-products still remain on the catalysts surface after the simple treatment by water and ethanol, which may ultimately lead to poisoning of catalysts. On the other hand, the TiO_2 nanoparticles may aggregate during the photocatalytic reactions. The morphology of MGO-Ce-TiO_2-10% after four cycles is shown in Fig. 11 (b). From the image, it can be seen that partial graphene nanosheets have been damaged into small pieces and can not provide large support for nanoparticles, resulting to an aggregation similar to bare Ce-TiO_2.

4. Conclusions

In summary, we have developed a simple and facile method for the preparation of magnetically separable MGO-Ce-TiO_2 nanostructured photocatalyst. Compared with TiO_2 or binary catalysts, the multiplex composite catalysts possessed high charge transferring properties of GO, superparamagnetic property of Fe_3O_4 and visible-light-activation of Ce-doped TiO_2. Our work verified the introduction of GO could efficiently improve the photocatalytic performance of Ce-TiO_2 in the degradation of antibiotic TC. Furthermore, the as-obtained samples could be removed from the treatment system by a magnet and displayed a good durability in several cycles. The degradation intermediate products were also studied by LC-MS analysis. On the basis of the identified intermediates, the photocatalytic degradation pathway of tetracycline was proposed. The as-obtained MGO-Ce-TiO_2 has a number of promising aspects, which can be applied in the treatment of medical sewage or pharmaceutical wastewater in future.

5. Acknowledgements

We are grateful for grants from National Science Funds for Creative Research Groups of China (No.51421006), Program for Changjiang Scholars and Innovative Research Team in University (No. IRT13061), National Science Fund for Distinguished Young Scholars (No. 51225901), the National Science Fundation of China for Excellent Young Scholars (No. 51422902), the Key Program of National Natural Science Foundation of China (No. 41430751)，the National Natural Science Foundation of China (No. 51579073)，Natural Science Foundation of Jiangsu

Province (BK20141417), Fundamental Research Funds for the Central Universities (2013B32114, 2013B14114) and PAPD.

References:

1 L. L. Ji, W. Chen, L. Duan, D. Q. Zhu, Mechanisms for strong adsorption of tetracycline to carbon nanotubes: a comparative study using activated carbon and graphite as adsorbents, Environ. Sci. Technol 43(2009) 2322-2327

2 Y. J. Wang, D. A. Jia, R. J. Sun, H. W. Zhu, D. M. Zhou, Adsorption and cosorption of tetracycline and copper(II) on montmorillonite as affected solution pH, Environ. Sci. Technol 42(2008) 3254-3259

3 Y. Gao, Y. Li, L. Zhang, H. Huang, J. J. Hu, S. M. Shah, X. G. Su, Adsorption and removal of tetracycline antibiotics from aqueous solution by graphene oxide, J. Colloid Interf. Sci 368(2012) 540-546

4 R. Andreozzi, V. Caprio, C. Ciniglia, M. Champdore, R. L. Giudice, R. Marotta, E. Zuccato, Antibiotics in the environment: occurrence in Italian STPs, fate, and preliminary assessment on algal toxicity of amoxicillin, Environ. Sci. Technol 38(2004) 6832-6838

5 J. Zilles. T. Shimada. A. Jindal, M. Robert, L. Raskin, Presence of macrolide-lincosamide-streptogramin B and tetracycline antimicrobials in swine waste treatment processes and amended soil, Water Environ. Res 77(2005) 57-62

6 J. C. Chee-Sanford, R. I. Aminov, I. J. Krapac, N. G. Jeanjean, R. I. Mackie, Occurrence and diversity of tetracycline resistance genes in Lagoons and groundwater underlying two swine production facilities, Appl. Environ. Microbiol 67(2001) 1494-1502

7 L. Aristilde, C. Marichal. J. M. Brendle, B. Lanson, L. Charlet, Interactions of oxytetracycline with a smectite clay: a spectroscopic study with molecular simulation,

Environ. Sci. Technol 44(2010) 7839-7845

8 H. Y. Sun, X. Shi, J. D .Mao, D. Q. Zhu, Tetracycline sorption to coal and soil humic acids: and examination of humic structural heterogeneity, Environ. Toxicol. Chem 29(2010) 1934-1942

9 L. S. Porubcan, C. J. Serna, J. L. White, S. L. Hem, Mechanism of adsorption of clindamycin and tetracycline by montmorillonite, J. Pharm. Sci 67(1978) 1081-1087

10 L. L. Ji, W. Chen, J. Bi, S. R. Zheng, Z. Y. Xu, D. Q. Zhu, P. J. Alvarez, Adsorption of tetracycline on single-walled and multi-walled carbon nanotubes as affected by aqueous solution chemistry, Environ. Toxicol. Chem. 29(2010) 2713-2719

11 A. L. P. F. Caroni, C. R. M. Lima, M. R. Pereira, J. L. C. Fonseca, Tetracycline adsorption on chitosan: a mechanistic description based on mass uptake and zeta potential measurements, Colloid. Surf., B 100(2012) 222-228

12 N. Oturan, J. Wu, H. Zhang, V. K. Sharma, M. A. Oturan, Electrocatalytic destruction of the antibiotic tetracycline in aqueous medium by electrochemical advanced oxidation processes: effect of electrode materials, Appl. Catal., B 140-141 (2013) 92-97

13 J. Wu, H. Zhang, N. Oturan, Y. Wang, L. Chen, M. A. Oturan, Application of response surface methodology to the removal of the antibiotic tetracycline by electrochemical process using carbon-felt cathode and DSA (Ti/RuO_2-IrO_2) anode, Chemosphere 87(2012) 614-620

14 I. Dalmazio, M. O. Almeida, R. Augusti, Monitoring the degradation of tetracycline by ozone in aqueous medium via atmospheric pressure ionization mass spectrometry, J. Am. Soc. Mass. Spectrom 18(2007) 679-687

15 Y. Wang, H. Zhang, J. H. Zhang, C. Lu, Q. Q. Huang, J. Wu, F. Liu, Degradation of tetracycline in aqueous media by ozonation in an internal loop-lift reactor, J. Hazard.

Mater 192(2011) 35-43

16 Y. Nosaka, T. Daimon, A.Y. Nosaka, Y. Murakami, Singlet oxygen formation in photocatalytic TiO_2 aqueous suspension, Phys. Chem. Chem. Phys 6 (2004) 2917-2918

17 A.Y. Nosaka, E. Kojima, T. Fujiwara, H. Yagi, H. Akutsu, Y. Nosaka, Photoinduced changes of adsorbed water on a TiO_2 photocatalytic film as studied by ^{1}H-NMR spectroscopy, J. Phys. Chem. B 107 (2003) 12042–12044

18 C. Reyes. J. Fernandez, J. Freer, M. A. Mondaca, C. Zaror, S. Malato, H. D. Mansilla, Degradation and inactivation of tetracycline by TiO_2 photocatalysis, J. Photochem. Photobiol., A 184(2006) 141-146

19 R. A. Palominos, M. A. Mondaca, A. Giraldo, G. Penuela, M. Perez-Moya, H. D. Mansilla, Photocatalytic oxidation of the antibiotic tetracycline on TiO_2 and ZnO suspensions, Catal. Today 144(2009) 100-105

20 X. D. Zhu, Y. J. Wang, R. J. Sun, D. M. Zhou, Photocatalytic degradation of tetracycline in aqueous solution by nanosized TiO_2, Chemosphere 92(2013) 925-932

21 X. L. Liu, P. Lv, G. X. Yao, C. C. Ma, P. W. Huo, Y. S. Yan, Microwave-assisted synthesis of selective degradation photocatalyst by surface molecular imprinting method for the degradation of tetracycline onto Cl-TiO_2, Chem. Eng. J 217(2013) 398-406

22 J. Yuan, Y. K. Lü, Y. Li, J. P. Synthesis and characterization of magnetic $TiO_2/SiO_2/NiFe_2O_4$ composite photocatalysts, Chem. Res. Chinese Universities 26 (2010) 278-282.

23 C. X. Wang, L. W. Yin, L. Y. Zhang, L. Kang, X. F. Wang, R. Gao, Magnetic $(\gamma\text{-}Fe_2O_3@SiO_2)_n$ @TiO_2 functional hybrid nanoparticles with active photocatalytic ability, J. Phys. Chem. C 113 (2009) 4008-4011

24 D. Beydoun, R. Amal, G. Low, S. McEvoy, Occurrence and prevention and photodissolution at the phase junction of magnetite and titanium dioxide, J. Mol. Catal. A: Chem 180 (2002) 193-200

25 Y. S. Chung, S. B. Park, D. W. Kang, Magnetically separable titania-coated nickel ferrite photocatalyst, Mater. Chem. Phys 86 (2004) 375-381

26 A. K. Geim, K. S. Novoselov, The rise of graphene, Nat. Mater 6(2007) 183-191

27 A. H. Castro Neto, F. Guinea, N. M. R. Peres, K. S. Novoselov, A. K. Geim, The electronic properties of graphene, Rev. Mod. Phys 81(2009) 109-162

28 J. Guo, S. Zhu, Z. Chen, Y. Li, Z. Yu, Q. Liu, J. Li, C. Feng, D. Zhang, Sonochemical synthesis of TiO_2 nanoparticles on graphene for use as photocatalyst, Ultrason. Sonochem 18(2011) 1082-1090

29 J. Shen, B. Yan, M. Shi, H. Ma, N. Li, M. Ye, One step hydrothermal synthesis of TiO_2-reduced graphene oxide sheets, J. Mater. Chem 21(2011) 3415-3421

30 C. Wang, M. Cao, P. Wang, Y. Ao, Preparation, characterization of CdS-deposited graphene-carbon nanotubes hybrid photocatalysts with enhanced photocatalytic activity, Mater. Lett 108(2013) 336-339

31 C. Wang, M. H. Cao, P. F Wang, Y. H. Ao, J. Hou, J. Qian, Preparation of a magnetic graphene oxide-Ag_3PO_4 composite photocatalyst with enhanced photocatalytic activity under visible light irradiation, J. Taiwan Inst. Chem. Eng 45(2014) 1080-1086

32 J. J. Xu, Y. H. Ao, D. G. Fu, A novel Ce, C-codoped TiO_2 nanoparticles and its photocatalytic activity under visible light, Appl. Surf. Sci 256(2009) 884-888

33 A. M. T. Silva, C. G. Silva, G. Drazic, Ce-doped TiO_2 for photocatalytic degradation of chlorophenol, J. L. Faria, Catal. Today 144(2009) 13-18

34 H. Zhang, X. J. Lv, Y. M. Li, Y. Wang, J. H. Li, P25-graphene composite as a high

performance photocatalyst, ACS Nano 4(2010) 380-386

35 T. Nguyen-Phan, V. H. Pham, E. W. Shin, H. D. Pham, S. Kim, J. S. Chung, E. J. Kim, S. H. Hur, The role of graphene oxide content on the adsorption-enhanced photocatalysis of titanium dioxide/graphene oxide composites, Chem. Eng. J 170(2011) 226-232

36 C. Wang, M. H. Cao, P. F. Wang, Y. H. Ao, J. Hou, J. Qian, Preparation of graphene-carbon nanotube-TiO_2 composites with enhanced photocatalytic activity for the removal of dye and Cr(VI), Appl. Catal. A 473(2014) 83-89

37 P. F. Wang, Y. H. Ao, C. Wang, J. Hou, J. Qian, A one-pot method for the preparation of graphene-Bi_2MoO_6 hybrid photocatalysts that are responsive to visible-light and have excellent photocatalytic activity in the degradation of organic pollutants, Carbon 50(2012) 5256-5264

38 J. C. Liu, H. W. Bai, Y. J. Wang, Z. Y. Liu, X. W. Zhang, D. D. Sun, Self-assembling TiO_2 nanorods on large graphene oxide sheets at a two-phase interface and their anti-recombination in photocatalytic applications, Adv. Funct. Mater 20(2010) 4175-7181

39 M. S. Zhu, P. L. Chen, M. H. Liu, Ag/AgBr/graphene oxide nanocomposite synthesized via oil/water and water/oil microemulsions: a comparison of sunlight energized plasmonic photocatalytic activity, Langmuir 28(2012) 3385-3390

40 J. G. Yu, J. Jin, B. Cheng, M. Jaroniec, A nobel metal-free reduced graphene oxide-CdS nanorod composite for the enhanced visible-light photocatalytic reduction of CO_2 to solar fuel, J. Mater. Chem. A 2(2014) 3407-3416

41 J. J. Guo, Y. Li, S. M. Zhu, Z. X. Chen, Q. L. Liu, D. Zhang, W. J. Moon, D. Song, Synthesis of WO_3@graphene composite for enhanced photocatalytic oxygen evolution from water, RSC Adv 2(2012) 1356-1363

42 P. Gao, Z. Y. Liu, M. H. Tai, D. D. Sun, W. J. Ng, Multifunctional graphene oxide-TiO_2 microsphere hierarchical membrane for clean water production, Appl. Catal. B 138-139(2013) 17-25

43 S. Y. Dong, J. Y. Sun, Y. K. Li, C. F. Yu, Y. H. Li, J. H. Sun, $ZnSnO_3$ hollow nanospheres/reduced graphene oxide nanocomposites as high-performance photocatalysts for degradation of metronidazole, Appl. Catal. B 144(2014) 386-393

44 H. Kim, S. Kim, J. Kang, W. Choi, Graphene oxide embedded into TiO_2 nanofiber: effective hybrid photocatalyst for solar conversion, J. Catal 309(2014) 49-57

45 Y. Yan, S. F. Sun, Y. Song, X. Yan, W. S. Guan, X. L. Liu, W. D. Shi, Microwave-assisted in situ synthesis of reduced graphene oxide-$BiVO_4$ composite photocatalysts and their enhanced photocatalytic performance for the degradation of ciprofloxacin, J. Hazard. Mater 250-251(2013) 106-114

46 Y. M. Ju, S. G. Yang, Y. C. Ding, C. Sun, A. Q. Zhang, L. H. Wang, Microwave-assisted rapid photocatalytic degradation of malachite green in TiO_2 suspensions: mechanism and pathways, J. Phys. Chem. A 112(2008) 11172-11177

47 J. F. Niu, S. Y. Ding, L. W. Zhang, J. B. Zhao, C. H. Feng, Visible-light-mediated Sr-Bi_2O_3 photocatalysis of tetracycline: kinetics, mechanisms and toxicity assessment, Chemosphere 93(2013) 1-8

48 R. Delepee, D. Maume, B. L. Bizec, H. Pouliquen, Preliminary assays to elucidate the structure of oxytetracycline's degradation products in sediments, determination of natural tetracyclines by high-performance liquid chromatography–fast atom bombardment mass spectrometry, J. Chromatogr. B 748(2000) 369-381

49 S. J. Jiao, S. R. Zheng, D. Q. Yin, L. H. Wang, L. Y. Aqueous photolysis of tetracycline and toxicity of photolytic products to luminescent bacteria, Chemosphere 73(2008) 377-382

Table captions:

Table 1 The BET surface area and the degradation data of TC for different samples under visible light irradiation.

Table 2 The identified of TC and its possible intermediates during the photodegradation process by MGO-Ce-TiO_2 under visible light irradiation.

Figure captions:

Fig. 1 XRD pattern of (a) Ce-TiO_2, (b) MGO-Ce-TiO_2-1%, (c) MGO-Ce-TiO_2-2%, (d) MGO-Ce-TiO_2-5% and (e) MGO-Ce-TiO_2-10%

Fig. 2 TEM images of (a) MGO and (b) MGO-Ce-TiO_2-10%

Fig. 3 Diffuse reflectance absorption spectra of the as-prepared sample

Fig. 4 Linear transform $\ln(C_0/C) = kt$ of the kinetic curves of TC photodegradation for different samples under visible light irradiation

Fig. 5 Histograms of the remaining concentration fraction of TC after adsorption by (a) Ce-TiO_2, (b) MGO-Ce-TiO_2-1%, (c) MGO-Ce-TiO_2-2%, (d) MGO-Ce-TiO_2-5%, (e) MGO-Ce-TiO_2-10% and (f) MGO-Ce-TiO_2-20%

Fig. 6 Photocurrents of different samples under intermittent visible light irradiation

Fig. 7 Schematic illustration of charge transfer in MGO-Ce-TiO_2 nanoparticles under visible light irradiation (The size of particles and atoms in this picture were not in agreement with fact)

Fig. 8 LC-MS analysis of TC and its intermediates in the photodegradation reaction in the presence of MGO-Ce-TiO_2

Fig. 9 Proposed possible pathways of photocatalytic degradation of TC under visible-light illumination in the presence of MGO-Ce-TiO_2

Fig. 10 Four cycling adsorption and photodegradation of TC over MGO-Ce-TiO_2-10%

Fig. 11 TEM images of MGO-Ce-TiO_2-10% after (a) magnetic separation and re-dispersing in water and (b) four cycles of TC photodecomposition

Table 1 The BET surface area and the degradation data of TC for different samples under visible light irradiation

Samples	Removal percent of TC (%)	Apparent rate constants k (min^{-1})	BET surface area (m^2 g^{-1})
Blank	2.16	---	---
P25	10.90	0.00209	---
Ce-TiO_2	29.31	0.00607	50.39
MGO-Ce-TiO_2-1%	35.48	0.00742	75.47
MGO-Ce-TiO_2-2%	46.13	0.01017	139.89
MGO-Ce-TiO_2-5%	63.12	0.01752	156.53
MGO-Ce-TiO_2-10%	82.92	0.03005	189.63
MGO-Ce-TiO_2-20%	72.74	0.02153	203.71

Table 2 The identified of TC and its possible intermediates during the photodegradation process by MGO-Ce-TiO_2 under visible light irradiation

Product	Retention time / min	Molecular weight	Proposed structure
TC	2.50	445	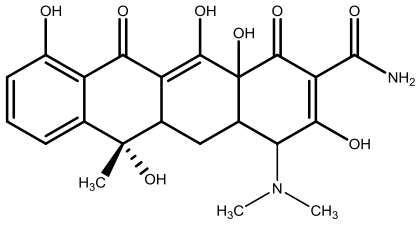
1	16.70	400	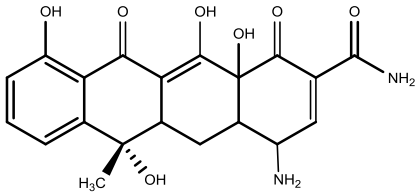
2	9.23	274	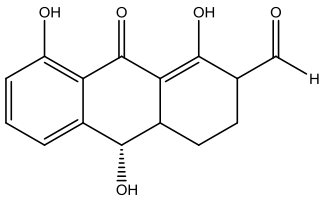
3	12.04	238	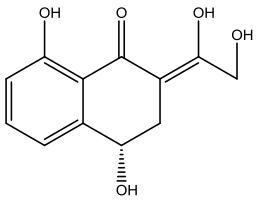
4	16.85	433	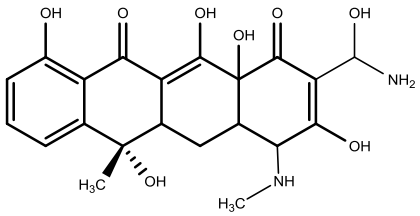
5	15.23	301	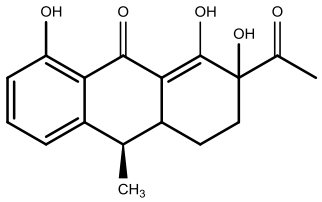
6	15.24	149	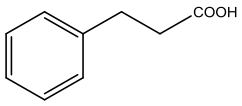

7	15.78	475	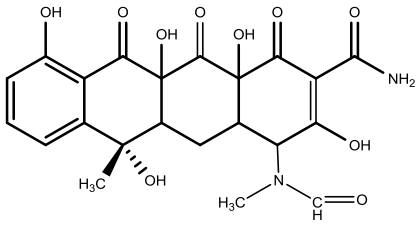
8	16.66	438	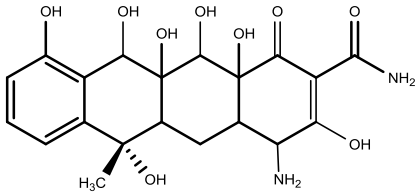
9	6.58	210	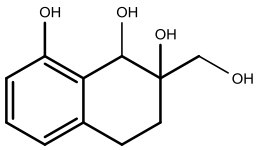

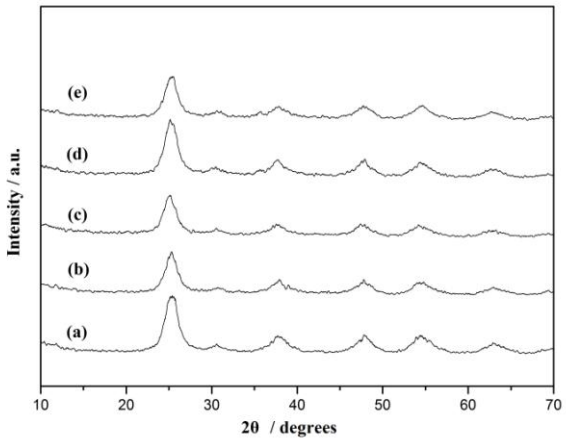

Fig. 1 XRD pattern of (a) Ce-TiO_2, (b) MGO-Ce-TiO_2-1%, (c) MGO-Ce-TiO_2-2%, (d) MGO-Ce-TiO_2-5% and (e) MGO-Ce-TiO_2-10%

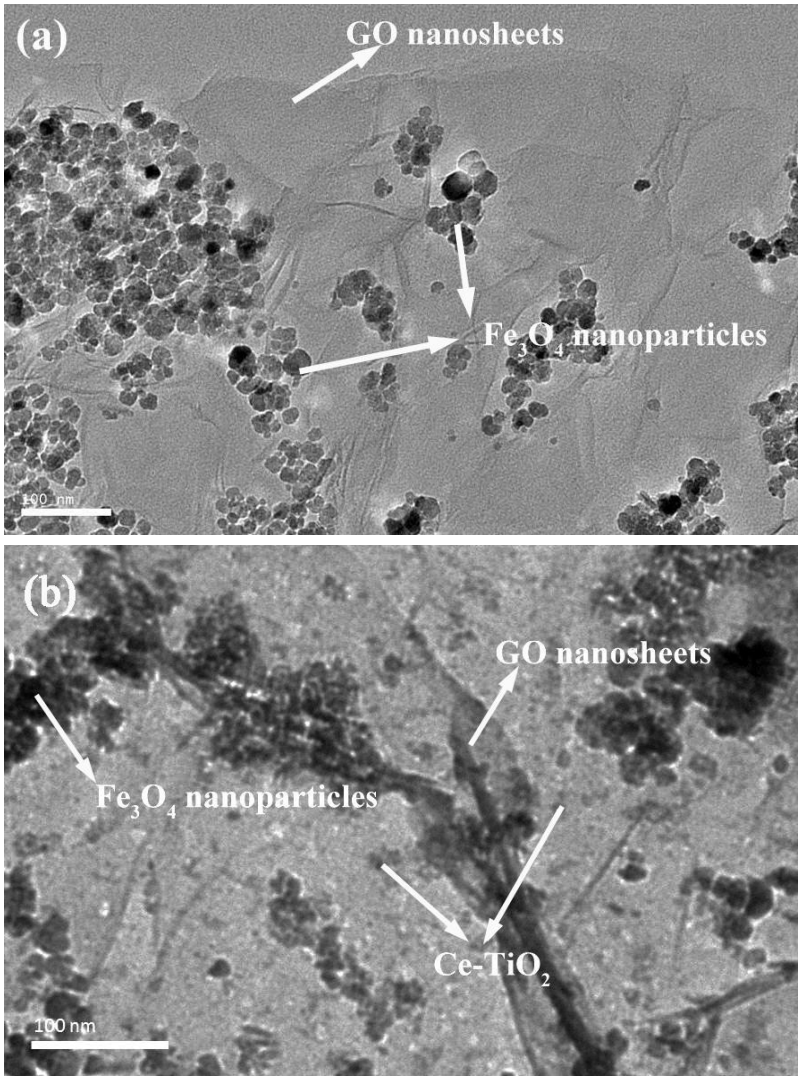

Fig. 2 TEM images of (a) MGO and (b) MGO-Ce-TiO_2-10%

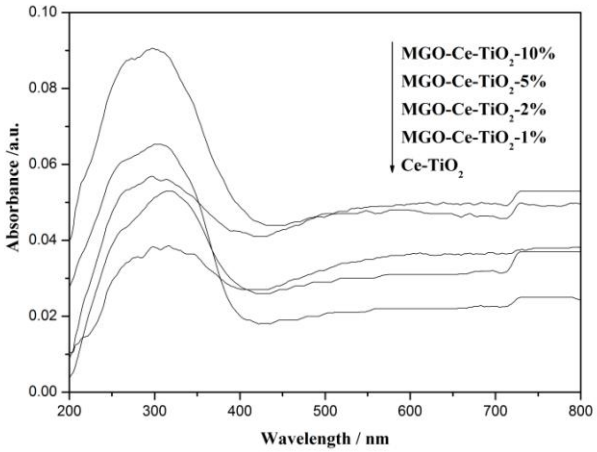

Fig. 3 Diffuse reflectance absorption spectra of the as-prepared samples

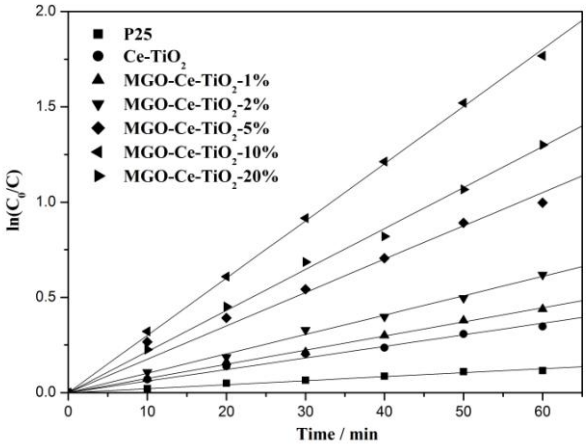

Fig. 4 Linear transform $\ln(C_0/C) = kt$ of the kinetic curves of TC photodegradation for different samples under visible light irradiation

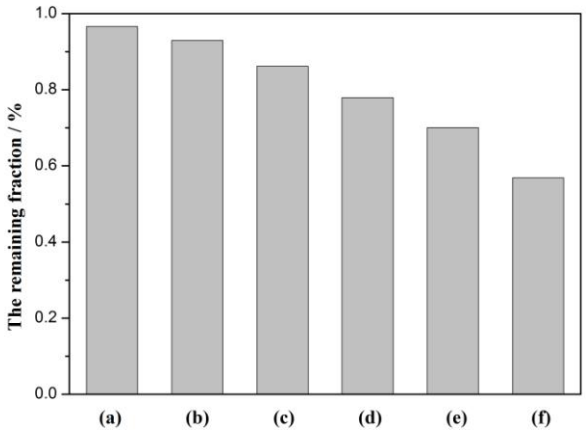

Fig. 5 Histograms of the remaining concentration fraction of TC after adsorption by (a) Ce-TiO_2, (b) MGO-Ce-TiO_2-1%, (c) MGO-Ce-TiO_2-2%, (d) MGO-Ce-TiO_2-5%, (e) MGO-Ce-TiO_2-10% and (f) MGO-Ce-TiO_2-20%

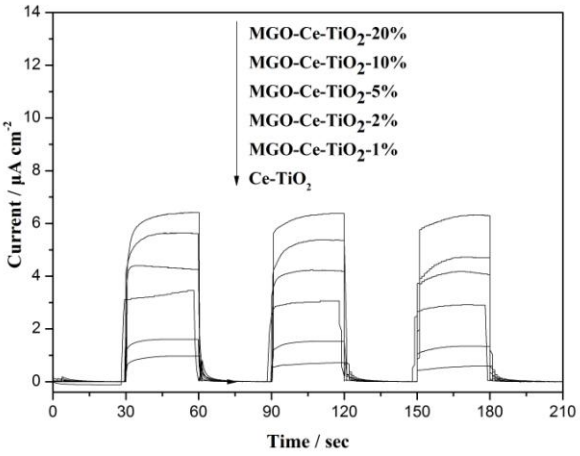

Fig. 6 Photocurrents of different samples under intermittent visible light irradiation

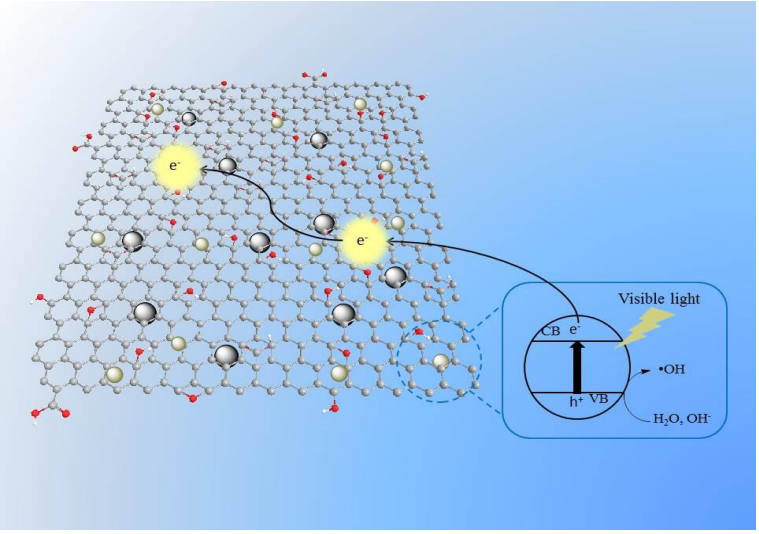

Fig. 7 Schematic illustration of charge transfer in MGO-Ce-TiO_2 nanoparticles under visible light irradiation (The size of particles and atoms in this picture were not in agreement with fact)

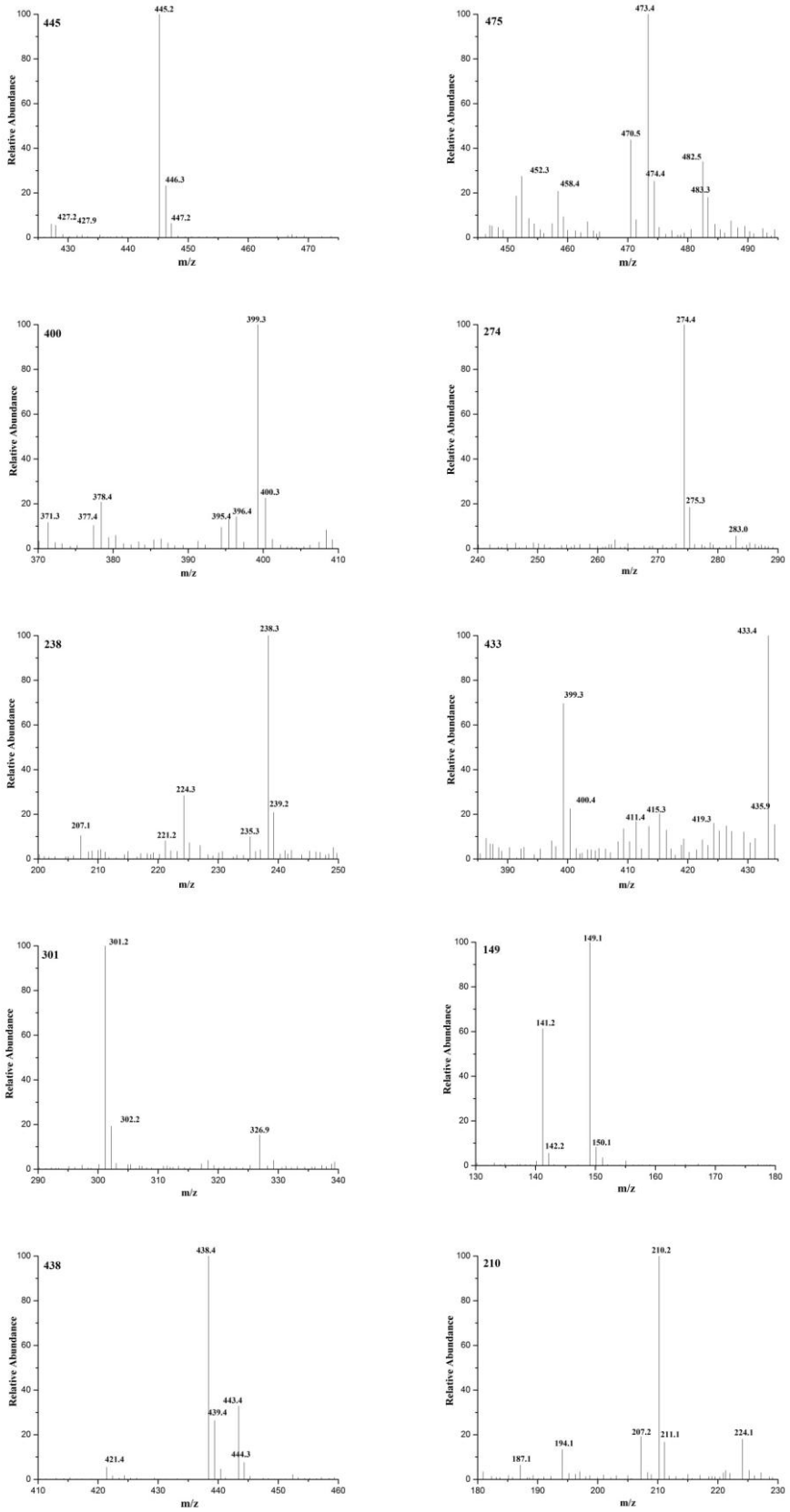

Fig. 8 LC-MS analysis of TC and its intermediates in the photodegradation reaction in the presence of MGO-Ce-TiO_2

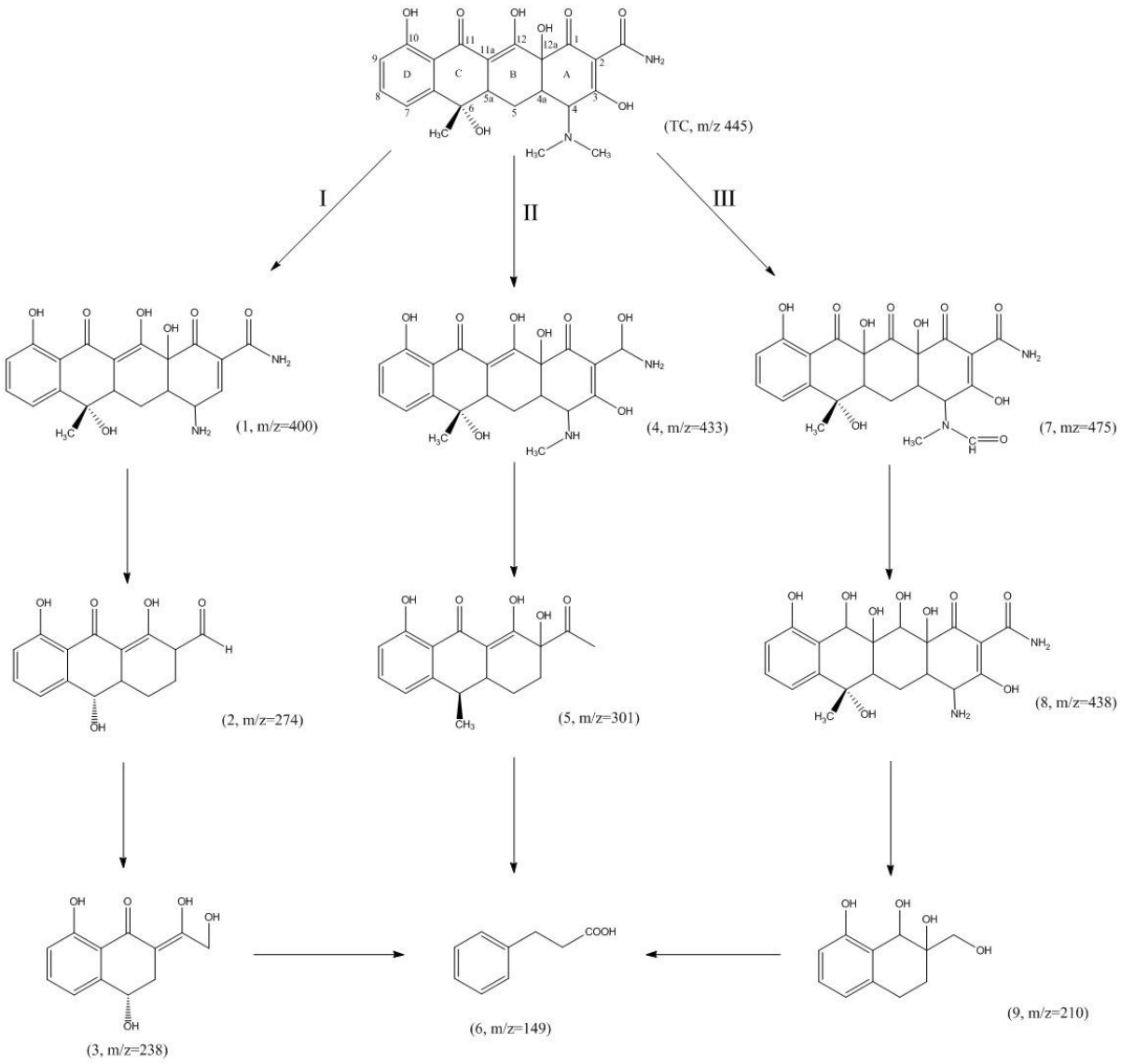

Fig. 9 Proposed possible pathways of photocatalytic degradation of TC under visible-light illumination in the presence of MGO-Ce-TiO_2

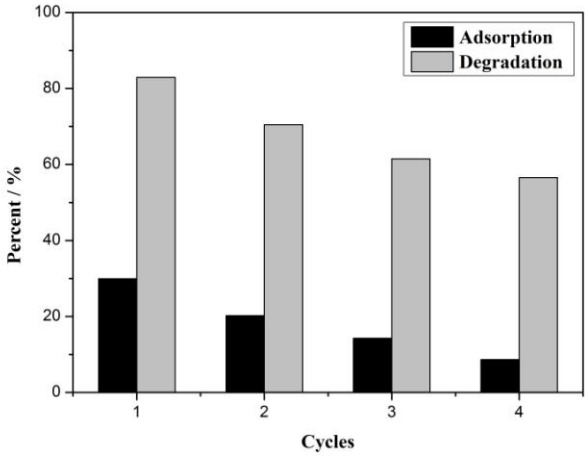

Fig. 10 Four cycling adsorption and photodegradation of TC over MGO-Ce-TiO_2-10%

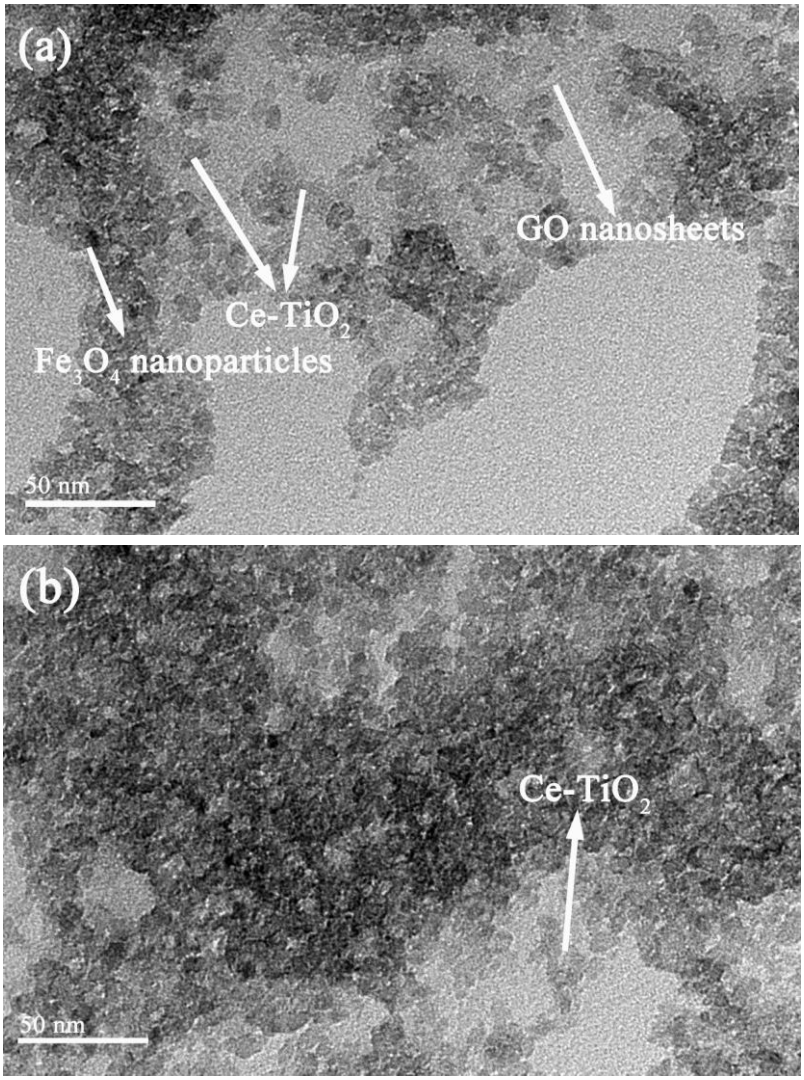

Fig. 11 TEM images of MGO-Ce-TiO_2-10% after (a) magnetic separation and re-dispersing in water and (b) four cycles of TC photodecomposition